# Numerical Characterization of Pressure Drop Across the Manifold of Turbine Casing Cooling System

# Numerical Characterization of Pressure Drop Across the Manifold of Turbine Casing Cooling System

**Riccardo Da Soghe**
e-mail: riccardo.dasoghe@htc.de.unifi.it

**Antonio Andreini**

Energy Engineering Department "S. Stecco,"
University of Florence,
50139, via S.Marta 3, Florence, Italy

*An array of jets is an arrangement typically used to cool several gas turbine parts. Some examples of such applications can be found in the impingement cooling systems of turbine blades and vanes or in the turbine blade tip clearances control of large aero-engines. In order to correctly evaluate the impinging jet mass flow rate, the characterization of holes discharge coefficient is a compulsory activity. In a previous work, the authors have performed an aerodynamic analysis of different arrays of jets for active clearance control; the aim was the definition of a correlation for the discharge coefficient ($C_d$) of a generic hole of the array. The developed empirical correlation expresses the ($C_d$) of each hole as a function of the ratio between the hole and the manifold mass velocity and the local value of the pressure ratio. In its original form, the correlation does not take in to account the effect of the hole length to diameter ratio (t/d) so, in the present contribution, the authors report a study with the aim of evaluating the influence of such parameter on the discharge coefficient distribution. The data were taken from a set of CFD RANS simulations, in which the behavior of the cooling system was investigated over a wide range of fluid-dynamics conditions (pressure-ratio = 1.01–1.6, t/d = 0.25–3). To point out the reliability of the CFD analysis, some comparisons with experimental data were drawn. An in depth analysis of the numerical data set has led to an improved correlation with a new term function of the hole length to diameter ratio.* [DOI: 10.1115/1.4007506]

## Introduction

Impingement with high velocity jets has become an established method for surface cooling or heating in a wide variety of processes and thermal control applications. The use of impingement jets for the cooling of modern aero-engine components is widespread, especially within the hot stationary parts. Since the cooling performance of impinging jets is very high, this method provides an efficient way to manage a component heat load when a sufficient pressure head and geometrical characteristics are available for its implementation. The cooling jets are usually arranged as arrays.

Aero-engine casing temperature control is a very effective way to reduce aerodynamic losses and specific fuel consumption due to blade tip clearance. Because of the significant variations of centrifugal and thermal loads occurring at different engine operating conditions, the tip clearance can be extremely variable; such dimensional variation may worsen engine performance and reduce the components' life span [1]. To overcome those issues, the Active thermal clearance control (ACC), generally based on impingement cooling, has been successfully introduced in several applications as described in Halila et al. [2], Beck and Fasching [3] and more recently by Justak and Doux [1]. In such systems, impinging jets are directed on the external turbine casing by means of a series of circumferential feeding pipes (Figs. 1 and 2) with the final aim of keeping the clearance between blade tip and casing as constant as possible at different engine operating conditions.

In order to correctly evaluate the impinging jet mass flow rate, the characterization of the holes discharge coefficient is a fundamental activity.

Contributed by the International Gas Turbine Institute (IGTI) of ASME for publication in the JOURNAL OF TURBOMACHINERY. Manuscript received June 28, 2012; final manuscript received August 9, 2012; published online March 25, 2013. Editor: David Wisler.

The discharge coefficient ($C_d$) is defined as the ratio of the actual mass flow rate through the hole and the isentropic flow rate. It summarizes all the losses that limit the actual mass flow rate through a hole: entry pressure losses, holes' interior losses due to friction, and exit losses. In order to evaluate the $C_d$, the actual mass flow rate is measured while the ideal mass flow is calculated under certain hypothesis. Assuming an isentropic one-dimensional expansion through an orifice from coolant pipe (secondary flow) total pressure ($P_t$) to the main flow (primary flow) static pressure ($P_d$), the obtained expression is:

$$C_d = \frac{\dot{m}}{P_t\left(\frac{P_d}{P_t}\right)^{\frac{\gamma+1}{2\gamma}}\sqrt{\frac{2\gamma}{(\gamma-1)RT_t}\left(\left(\frac{P_t}{P_d}\right)^{\frac{\gamma-1}{\gamma}}-1\right)}\frac{\pi}{4}d^2} \quad (1)$$

Many parameters may influence the discharge coefficient [4]: geometrical, as hole shape, hole angle, space between holes, length to diameter ratio, etc., and fluid-dynamics, as the pressure ratio across the hole, Reynolds and Mach number of the two cross-flows, and inside the hole, etc. For this reason, several studies have been carried out on different geometries of holes subjected to a wide range of fluid-dynamics conditions; an extensive review can be found in Hay and Lampard [5].

More recently, Gritsch et al. [6] investigated the behavior of a single hole of large diameter (10 mm); they proposed a method for correlating the discharge coefficients, assuming that pressure losses inside the hole and those related to the hole entry and exit are independent. Internal losses are found to be dependent on the pressure ratio across the hole, while the entry and exit losses depend on the jet to cross-flow momentum ratio. With these hypotheses, Gritsch et al. [7] studied the influence of the internal cross-flow on shaped holes, while Robwbury et al. [8] proposed a method to quantify the influence of external cross-flow on $C_d$. In a more recent contribution, Gritsch et al. [9] performed several experiments, analyzing the behavior of $C_d$ with varying internal

  

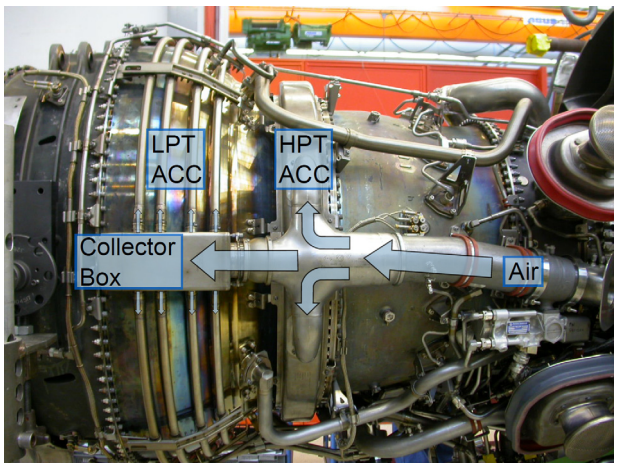


**Fig. 1 ACC system, Ahmed et al. [18]**

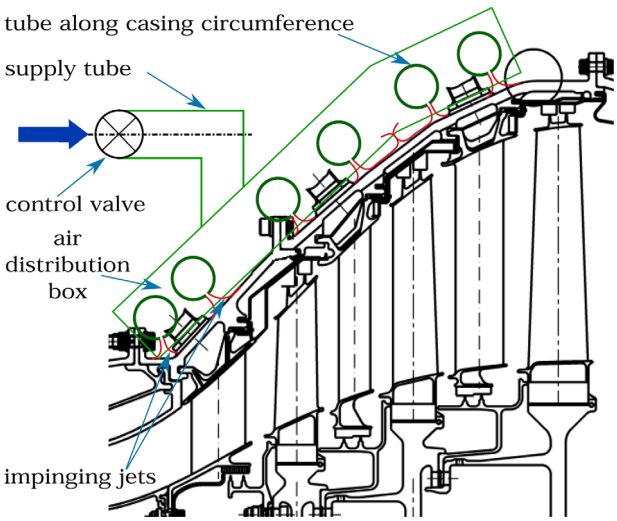


**Fig. 2 Scheme of a LPT ACC system, Ahmed et al. [19]**

and external cross-flow conditions and geometrical angles and using the jet-to-cross-flow momentum ratio to reduce data.

According to Thole et al. [10], the assumption that the source of pressure losses is independent seems not to be universally valid: the hole must be sufficiently long to permit the distortion of the inlet flow caused by the cross-flow decay before the outlet is reached. From the evidence of Hay et al. [11], $t/d = 6$ is certainly sufficient.

Quite interesting results on jet array impingement systems have been recently pointed out by Goodro and coworkers [12–16]. The authors reveal that the holes' discharge coefficient is affected by both jet Reynolds and Mach number.

Andreini and coworkers [17] performed a series of CFD RANS simulation on an aero-engine combustor liner. Final results of this work were the definition of a correlation for the discharge coefficient of the single effusion hole of the array expressed as a function of the ratio between the hole and the annulus Reynolds number, the inlet flow function, and the velocity head ratio of the hole.

More recently, Ahmed et al. [18,19] performed some numerical simulation of the flow in a short tube section of an ACC system for a low pressure turbine aimed at the prediction of impingement jet characteristics in form of discharge coefficients, local and spatially averaged Nusselt numbers and heat transfer coefficients. The length-to-diameter ratio of the sharp-edged cylindrical holes, ranged from 0.25 to 2, was also accounted. The authors pointed out that the $C_d$ varies across the feeding tube and it is affected strongly by the length-to-diameter parameter.

In one of their last contributions, Andreini and Da Soghe [20] presented a correlation for the $C_d$ of impingement holes located on cylindrical manifolds. The work aimed at a general characterization of the losses of the impingement cooling arrangements for ACC systems, allowing for the isolation of the effects of the main fluid-dynamics parameters. The study led to the development of an empirical correlation that expresses the $C_d$ of each impingement hole as a function of the ratio between the hole and the manifold mass velocity and the local value of the pressure ratio. In its original form, the correlation is valid just in case of hole length-to-diameter ratio equal to 2. The last evidence represents the main limitation of the developed correlation. In order to improve the original correlation, the data set has been extended in the present work by including the effect of length-to-diameter ratio, and an updated expression for the correlation is obtained and discussed. In particular, a new set of CFD computations was carried out on several cylindrical manifold geometries with different holes length-to-diameter ratio and with different holes axial displacements.

## Description of Geometries and Test Matrix

This work aims at a general characterization of the losses of the impingement cooling arrangements for ACC systems, allowing to isolate the effects of the main fluid-dynamics and geometrical parameters. Such systems are usually composed of hole arrays drilled at 90 deg with respect to the feeding pipe axis and the spent jets evolve in a low velocity environment.

Recovering the approach described in the prior work of the authors (Andreini and Da Soghe [20]), an extensive numerical analysis is carried out on an isolated cylindrical manifold domain, for a wide range of operating conditions with different cooling holes geometries. The same geometrical layout was also considered in a dedicated test rig described in Da Soghe et al. [21], where pressure losses and discharge coefficients are obtained by measurements.

The manifolds considered in this work (Fig. 3) are fed through one side while the other side is closed (i.e. the entire mass flow rate exits throughout the holes). The tubes' length is $L = 400$ mm with holes diameter $d = 1$ mm. In this work, several geometrical arrangements have been considered taking in to account the effects of holes length-to-diameter ratio ($t/d$), holes number and holes axial displacement. All the simulated geometries are reported in Table 1. The rationale for these configurations will be clear through the text.

As mentioned above, the numerical domain, shown in Fig. 4, consists in a single feeding manifold that discharges in a plenum whose overall dimensions are $500 \times 500 \times 500$ mm. As the holes discharge in a quiescent environment, the effect of the external flow on the holes $C_d$ is not considered in this work. This assumption can be safely accepted taking into account that actual ACC cooling jets are usually injected in low velocity cross flow ($Ma \ll 0.1$ as confirmed by the investigations reported in Da Soghe and coworkers [22] and also by Gritsch et al. [9]), sufficiently far from cooled wall to avoid the effects of stagnation point and heat transfer on jet discharge losses.

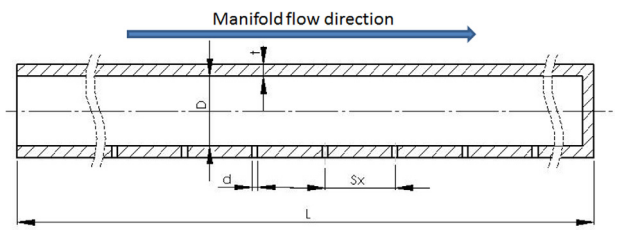


**Fig. 3 Tested geometries**

Table 1 Impingement tubes arrangement

| Geom. label | D (mm) | $t/d$ | $S_x/d$ | Holes number |
|---|---|---|---|---|
| A | 12 | 2 | 1.5 | 134 |
| B | 6 | 3 | 3 | 34 |
| C | 6 | 2.5 | 3 | 34 |
| D | 6 | 2 | 3 | 34 |
| E | 6 | 2 | 1.5 | 34 |
| F | 6 | 1 | 3 | 34 |
| G | 6 | 1 | 1.5 | 34 |
| H | 6 | 0.5 | 3 | 34 |
| I | 6 | 0.25 | 3 | 34 |

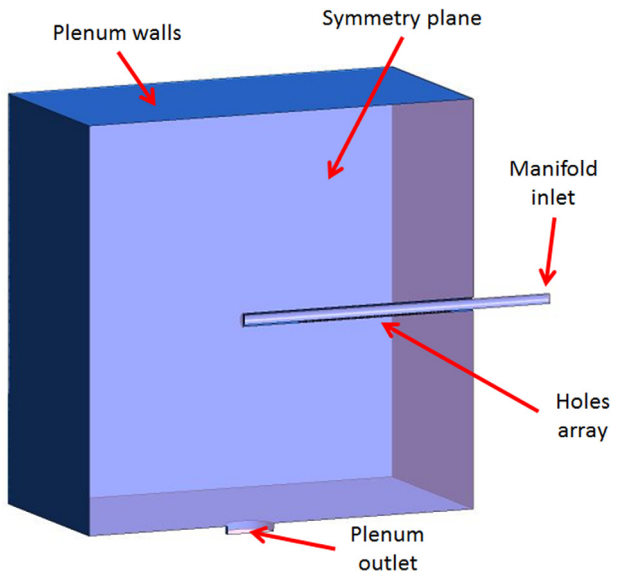


Fig. 4 Numerical domain

Table 2 Operating conditions

| Geom. label | $\beta$ | Pipe inlet $Re$ |
|---|---|---|
| A | 1.01, 1.12, 1,22, 1.3 | $2 \cdot 10^4 \div 6 \cdot 10^4$ |
| B | 1.08, 1.6 | $2 \cdot 10^4 \div 6 \cdot 10^4$ |
| C | 1.08 | $2 \cdot 10^4$ |
| D | 1.08, 1.6 | $2 \cdot 10^4 \div 6 \cdot 10^4$ |
| E | 1.08, 1.3, 1.6 | $2 \cdot 10^4 \div 6 \cdot 10^4$ |
| F | 1.09, 1.6 | $2 \cdot 10^4 \div 6 \cdot 10^4$ |
| G | 1.09, 1.6 | $2 \cdot 10^4 \div 6 \cdot 10^4$ |
| H | 1.1, 1.4, 1.65 | $2 \cdot 10^4 \div 6 \cdot 10^4$ |
| I | 1.1, 1.65 | $2 \cdot 10^4 \div 6 \cdot 10^4$ |

The operating conditions considered for each geometry are reported in Table 2.

To calculate the $C_d$, the upstream fluid-dynamic quantities were calculated above the inlet of each hole, on the centerline of the manifold, while the discharge static pressure was evaluated within the plenum. Both the isentropic mass flow rate and the local pressure ratio were evaluated using static quantities.

From the postprocessing of the CFD results, values of discharge coefficient for each hole were extracted for each simulation, allowing to get a data set of more than 1000 $C_d$ evaluations.

## CFD Modeling

**Numerical Tools and Meshing Criteria.** CFD steady state calculations have been performed with the commercial 3D Navier–Stokes solver Ansys® CFX v.12.

A symmetry condition has been imposed at the facility symmetry plane while no-slip and adiabatic conditions have been applied on solid surfaces. The pressure boundary condition has been imposed at the outlet while mass flow rates were fixed at the inlet.

Compressibility effects have been taken into account and a 2nd order Upwind advection schemes have been used. The fluid (air) has been modeled as ideal gas and the properties of specific heat capacity, thermal conductivity and viscosity have been assumed as constants.

The energy equation has been solved in terms of total temperature and viscous heating effects have been accounted for.

The k-$\omega$-SST turbulence model, in its formulation made available by the CFD solver, has been used in conjunction with an automatic wall treatment in the near wall regions. The automatic wall treatment consists in a formulation which automatically switch from wall-functions to a low-Re near wall formulation as the mesh $y^+$ lies below 1. Further details about the turbulence model and the near wall treatment can be found within the code's guide [23].

The convergence of solutions has been assessed by monitoring domain mass imbalance (below 0.001%) and residuals (below $10^{-7}$). Furthermore the runs have been stopped when the pressure level and other physical quantities on different locations, reached a steady state.

The mesh generation tool Ansys® ICEM-CFD has been used to generate a tetrahedral cell mesh. A number of grid sensitivity tests have been carried out in order to ensure mesh independent solutions. Some findings of this analysis are shown in Figs. 6 and 9 where the results obtained by the use of the standard mesh selected for the geometry A (3 Me and $y^+ > 15$), have been compared with the predictions evaluated using a more refined mesh (8 Me and $y^+ > 5$); a comparison between the two meshes is reported in Fig. 5. The refined mesh has been generated reducing the grid $y^+$ values within the holes and refining the grid size just close to the holes. Far away from the holes, the grids are the same. Bearing in mind that the original mesh counts $3 \times 10^6$ elements and the refined one $8 \times 10^6$ elements, this means that the elements for each hole are, in the refined mesh, more than double of those related to the standard mesh.

As shown by the figures, the two meshes provide a rather similar distribution of the mass flow rates across the 134 holes and the same static pressure distribution within the manifold. The same mesh sensitivity analysis has been repeated for the geometry labeled H (Fig. 7). In this case the mesh has been generated, and then refined, with the same criteria adopted for the geometry A. Thus, it can be assumed that mesh independent solutions are achieved using the standard grids. Similar conclusions have been pointed out for the other operating conditions and other geometries analyzed in this work.

In order to investigate the sensitivity to turbulence modeling, the baseline BSL Reynolds Stress Model made available by the solver (for further details about the BSL model please refer to Ref. [23]) has been considered and the results of its predictions have been compared the those obtained through the $k - \omega - SST$. Some findings of this analysis are shown in Figs. 8 and 9. The figures reveal that the two turbulence models provide a similar distribution of the mass flow rates across the manifold and the same static pressure distribution from the inlet to the end cap of the tube.

**Validation of CFD Methodology.** A preliminary validation of the numerical setup was carried out by the authors in a previous work where the experimental analysis performed by Gritsch et al. [9] was successfully replicated using a similar CFD methodology (Andreini et al. [17]).

In order to further assess the CFD predictions reliability, a comparison between the pressure profiles evaluated within the supply pipe and the related dedicated experimental data has been drawn. The experimental data have been established through an extensive

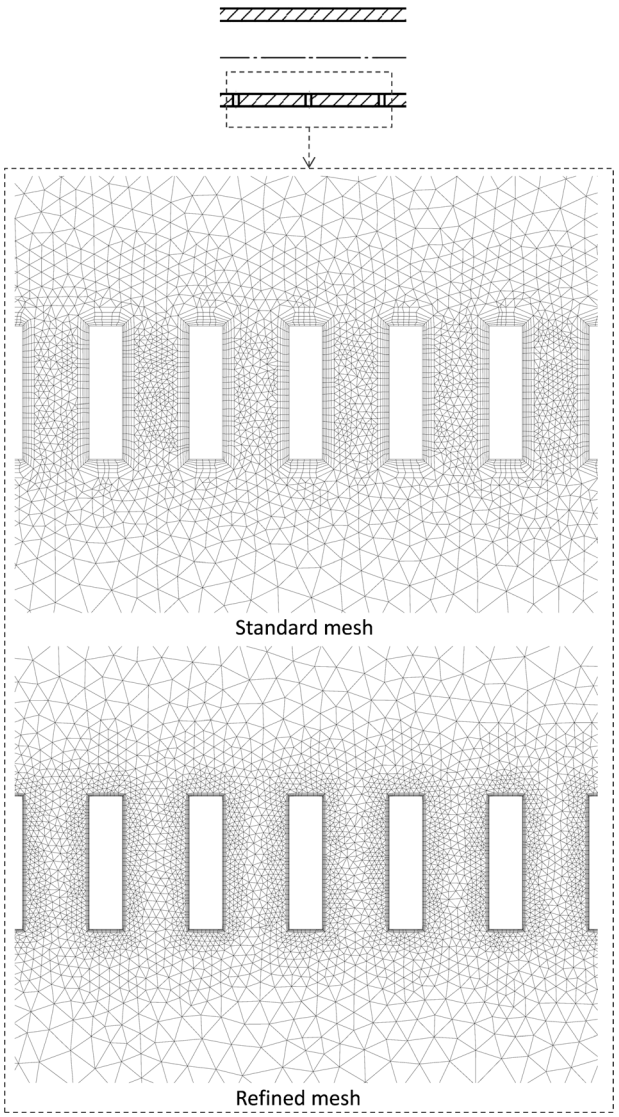


**Fig. 5 Standard and refined CFD mesh for geometry A**

experimental campaign performed in the already mentioned dedicated test rig [21]. The experiments have considered several geometries and have provided reliable evaluation of the pressure profiles within the manifolds. Within the test bed, the pressure

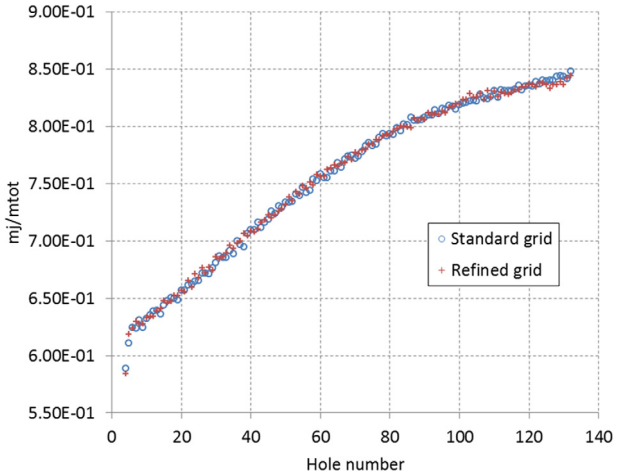


**Fig. 6 CFD mesh sensitivity: geometry A mass flow rate split (%) in case of $\beta = 1.12$**

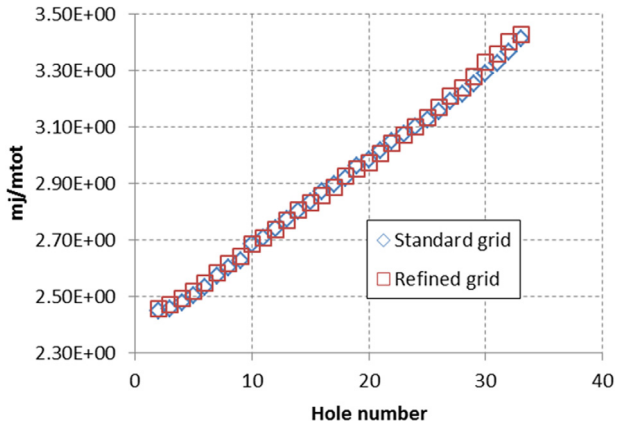


**Fig. 7 CFD mesh sensitivity: geometry H mass flow rate split (%) in case of $\beta = 1.1$**

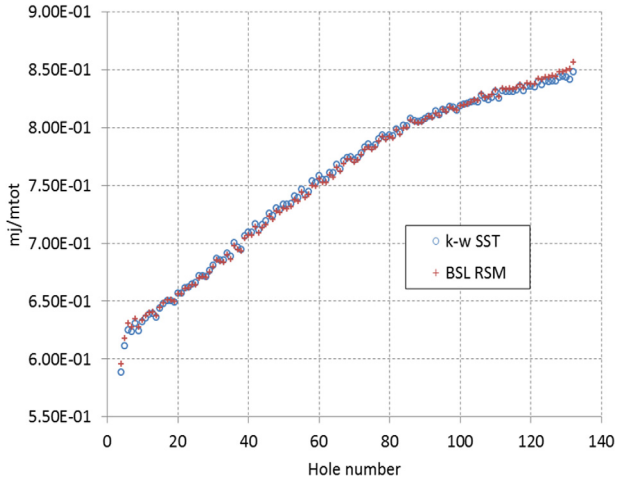


**Fig. 8 CFD turbulence modeling sensitivity: geometry A mass flow rate split (%) in case of $\beta = 1.12$**

levels have been measured through five pressure taps along the manifold that result in five measure points (MP) (see the upper part of Fig. 9). For further details regarding the experimental analysis, please refer to Da Soghe et al. [21].

Figure 9 reports the pressure profiles evaluated for the geometry A scaled by the total pressure at the MP1 evaluated by the

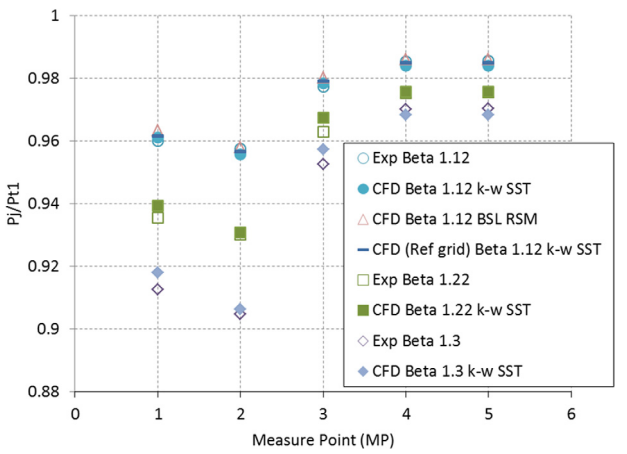


**Fig. 9 Comparison between CFD and experimental results in terms of manifold centerline pressure distribution—geometry A**

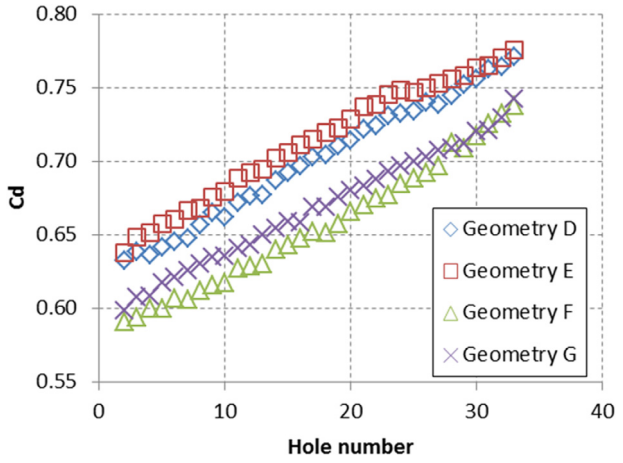


**Fig. 10 Discharge coefficient distribution: geometry D, E, F, G $\beta = 1.1$**

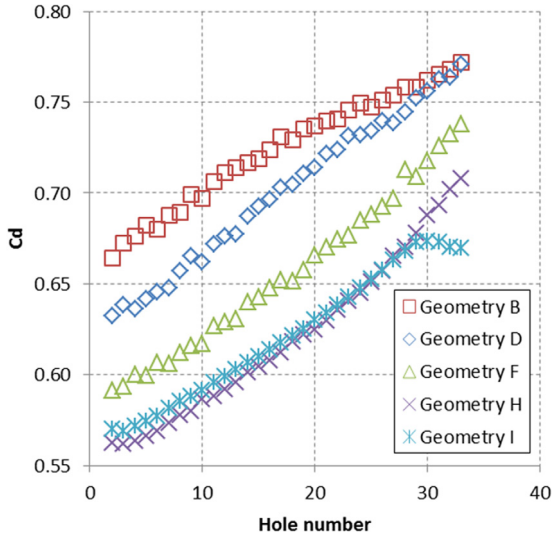


**Fig. 11 Discharge coefficient distribution: geometries B, D, F, H, I, $\beta = 1.1$**

experiments. In a wide range of operating conditions (i.e. in a wide range of overall $\beta$ ratio), the CFD predictions are in fairly good agreement with the experimental data. Similar conclusions have been drawn for other geometries analyzed in this work. Considering that the static pressure profile is closely related to the mass flow rate distribution across the holes, the CFD can be considered a reliable tool for the system discharge behavior prediction and it can be safely used to extend experimental test matrix.

## Results

**Effects of $S_x/d$ Parameter on the Holes $C_d$.** The effects of the holes spacing on the discharge coefficient have been analyzed by focusing on geometries labeled D, E, F, and G. For these geometries, trends of $C_d$ plotted versus the increasing hole number are presented in Fig. 10. The first and the last holes are not considered because their behavior is affected by the border effects and differs significantly from the others.

The impact of the holes spacing is appreciable for the first manifold holes and becomes less appreciable when approaching the manifold end. For each $t/d$ ratio considered, the geometries with the higher holes pitch shows lower values of the local discharge coefficient. This last evidence could be motivated by observing that the increase of the $S_x/d$ parameters leads to a cross-flow much more aligned to the manifold axis. The increase of the flow angle at the hole inlet leads to stronger inlet losses and then lower values of discharge coefficient are observed. These effects are purely related to the jet to cross flow momentum ratio and then, as confirmed by Fig. 10, they become negligible when approaching the manifolds end. This behavior seems to not be affected by the holes length-to-diameter ratio. The above described phenomenon is, however, quantitatively comprised in the range of 4% concerning the CFD evaluated discharge coefficient. As the last evidence is also true for the other operating conditions and geometries considered here, the $S_x/d$ parameter will not be accounted for in the definition of hole $C_d$ correlation.

**Effects of the $t/d$ Ratio on the Holes $C_d$.** Trends of $C_d$ plotted versus the increasing hole number are presented in Fig. 11 for the geometries labeled B, D, F, H, and I in case of $\beta = 1.1$. Looking at the results obtained for the geometries D, F, and H (i.e. for a $t/d$ ratio ranging from 2 to 0.5), the plot shows how the $C_d$ increases roughly linearly towards the end of the manifold, indicating a direct relation with the coolant mass flow left in the annulus. Furthermore, from the figure emerges that, for the mentioned geometries, the increase of the $t/d$ ratio leads to an increase of the holes discharge coefficient. As shown in the Fig. 12, flow separation immediately took place at the upper corners of the holes forming large recirculation zones at the walls and a vena contracta was observed. For the small length-to-diameter ratios ambient air was additionally sucked into the separation zones. Increasing the $t/d$ ratio up to 3 led to reattachment of the flow. No surrounding air was sucked into the bores and the vena contracta formed was expanded until disappearing within the holes. As the $t/d$ ratio increases it decrease the fluid velocity at the exit of the hole resulting in a reduction of the pressure losses.

The geometries B and I show different behaviors. Regard the geometry B (i.e., for $t/d = 3$) the predicted discharge coefficients are generally higher than those calculated in the case of $t/d = 2$ while, approaching the end of the feeding pipe, the discrepancy between the evaluated $C_d$ become smaller. The explanation of such phenomenon could be found by observing that, approaching the end of the feeding pipe, the manifold flow momentum decrease and then the pipe tend to act as a plenum for the last holes of the array. In such configuration Lichtarowicz et al. [24] shows that, in term of $C_d$, holes with $t/d = 3$ behaves as hole with $t/d = 2$. In the case of $t/d = 0.25$ (geometry labeled I), the predicted discharge coefficients are close to those related to geometry H for the major part of the holes while, approaching the end of the manifold, the $C_d$ remains constant as already pointed out also by Ahmed et al. [18,19]. For these reasons, the geometry I was not considered for the definition of the improved correlation.

Figure 13 shows the $C_d$ distribution over the *MVR* parameter for the geometries B, F, and H (i.e. $t/d$ equal to 3, 1, and 0.5, respectively) in case of overall $\beta = 1.1$. The figure confirms what already pointed out by the authors in the past (see Andreini and Da Soghe [20]): for each hole length-to-diameter ratio, the discharge coefficient is quite sensible to the mass flow velocity ratio for *MVR* values below 5 circa, while it is quite independent from this parameter for *MVR* high values. This confirms that the influence of the internal cross flow on the $C_d$ is only relevant for low values of *MVR* for each $t/d$ ratio considered in present contribution. As reported by Andreini and Da Soghe [20], the reduction of the discharge coefficient at low MVR region could be directly related to the increase of the flow angle (measured from the holes axis) at the hole inlet section with the decrease of the MVR parameter. The increase of the flow angle leads to a more severe separation zone. As the hole has a circular shape it is expected that the vena-contracta area changes in a steeper way than a simple linear function of the separated flow region extension (i.e. with the flow angle at the inlet of the hole). This can explain why the $C_d$ shows the logarithmic like behavior here reported. From Fig. 13, it can be also observed to that in the low MVR region the changes

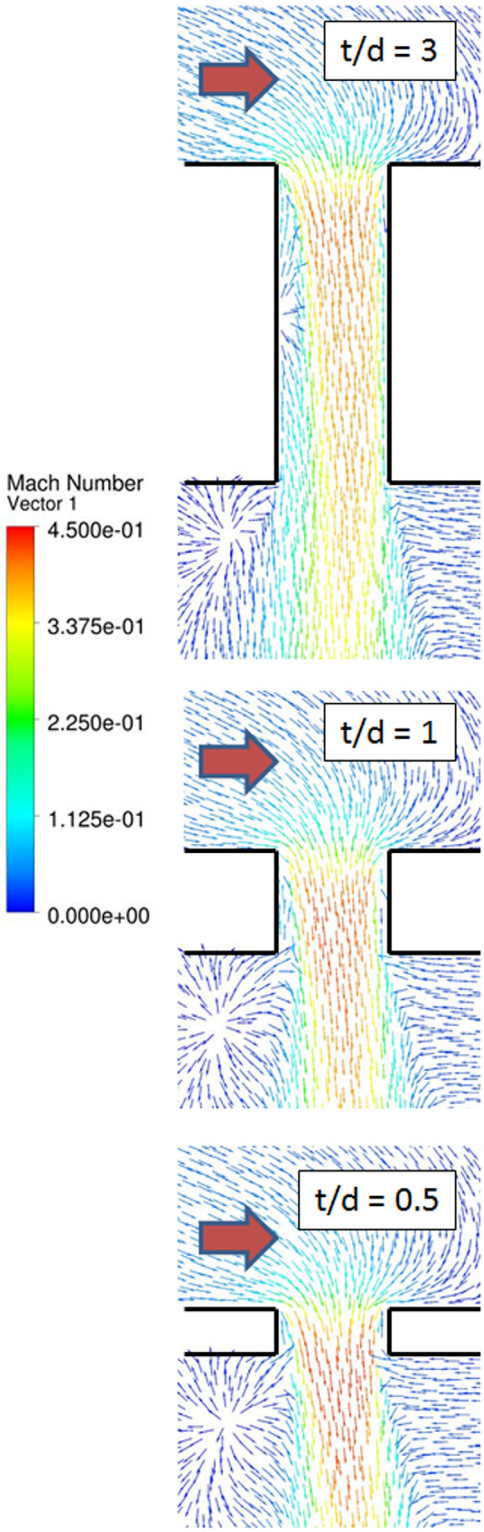


**Fig. 12 Holes separation zones: normalized vector plot**

in the predicted $C_d$ are less steep in case of low $t/d$ ratio. The last statement could be motivated observing that, in case of high $t/d$ ratio, the vena-contracta is located completely inside the holes extent making the effects of the flow angle at the hole inlet more prominent.

**Data Reduction.** From Andreini and Da Soghe [20], in order to lump the effect of the operating condition in the $C_d$, scaled the

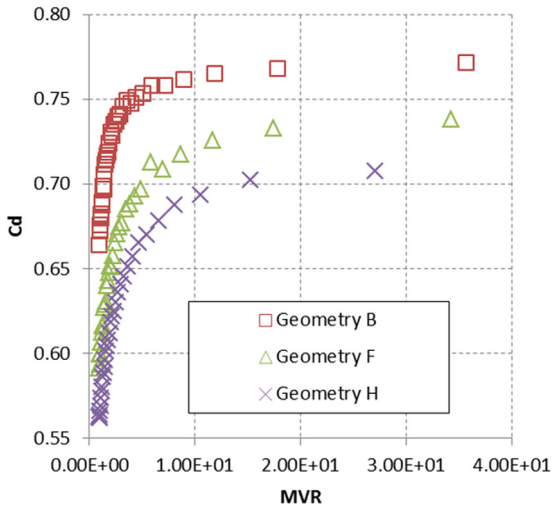


**Fig. 13 Discharge coefficient over *MVR* parameter distribution: geometry B, F, H, $\beta = 1.1$**

calculated discharge coefficients with the hole local $\beta_L$ ratio elevated to a suitable constant:

$$C_d^* = \frac{C_d}{\beta_L^\alpha} \tag{2}$$

In case of $t/d = 2$ it was found that the best fit is obtained with $\alpha = 0.19$ (Andreini and Da Soghe [20]). Figure 14 shows that $\alpha = 0.19$ is not able to properly lump the $C_d$ profiles for different hole length-to-diameter ratios, meaning that the $\alpha$ coefficient should be expressed as a function of the $t/d$ parameter.

$$\alpha = f\left(\frac{t}{d}\right) \tag{3}$$

Considering all the geometries and the related operating conditions, the expression of $\alpha$ that better scaled the $C_d^*$ has been found as second order polynomial function in term of $t/d$:

$$\alpha = 0.0124\left(\frac{t}{d}\right)^2 - 0.117\frac{t}{d} + 0.379 \tag{4}$$

When considering different geometries, the effect of the $t/d$ ratio on the $C_d^*$ parameter is clearly visible looking at Fig. 15. In order

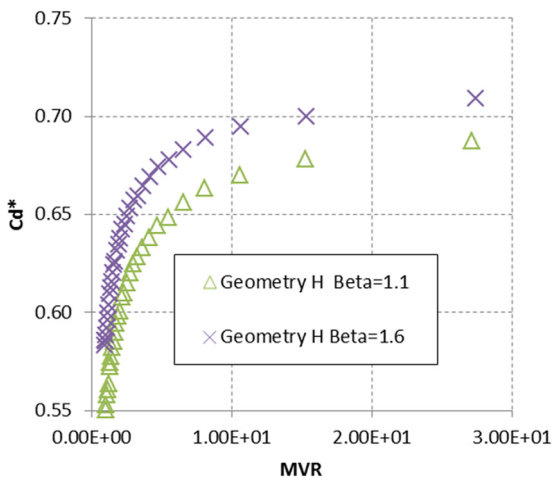


**Fig. 14 $C_d^*$ over *MVR* parameter distribution: case H, $\alpha = 1.19$**

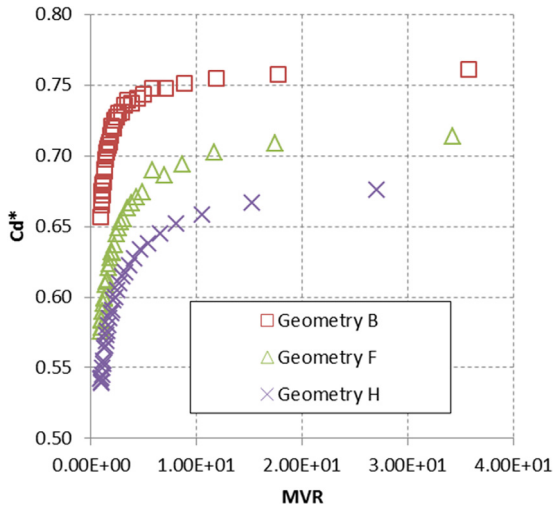


**Fig. 15 $C_d^*$ over *MVR* parameter distribution: case B, F, H, $\alpha$ function of $t/d$ ($\beta = 1.1$)**

to eliminate the dependency on the $t/d$ ratio, the $C_d^*$ has been scaled by a suitable function:

$$C_d^{**} = \frac{C_d^*}{g\left(\frac{t}{d}\right)} \tag{5}$$

where,

$$g\left(\frac{t}{d}\right) = -0.0204\left(\frac{t}{d}\right)^2 + 0.129\frac{t}{d} + 0.826 \tag{6}$$

Figure 16 shows the $C_d^{**}$ parameter as a function of the *MVR* parameter evaluated for all the geometries considered in this work. The figure reveals that the obtained numerical data collapse quite well and so it is assumed that $C_d$ can be expressed as a function of the local pressure ratio, the hole length-to-diameter ratio and the local *MVR*:

$$C_d = f(\beta_L, t/d, MVR) \tag{7}$$

The generic hole $\beta_L$ ratio allows a local correction of the value predicted using the *MVR* parameter, while the $t/d$ ratio introduces the correction related to the impinging system geometry, increasing the global accuracy of the correlation. In order to separate the

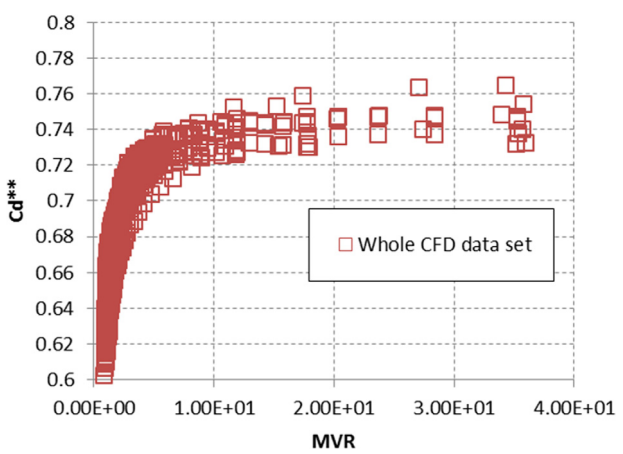


**Fig. 16 $C_d^{**}$ over *MVR* parameter distribution: whole CFD data set (i.e. all geometries and related operating conditions)**

**Table 3 Correlation coefficients**

| Coefficient | Value |
|---|---|
| $c_1$ | 0.745 |
| $c_2$ | − 1262 |
| $c_3$ | 3.1 |
| $c_4$ | −8 |
| $\gamma$ | 0.1124 |

effects of the cross flow on the $C_d$, the discharge coefficient of the single hole will be expressed as a product of two terms:

$$C_d = C_{d\_noCrFlow} \cdot C_{d\_IntCrFlow} \tag{8}$$

where

$$C_{d\_noCrFlow} = c_1 \cdot \beta_L^{\alpha} \cdot g\left(\frac{t}{d}\right) \tag{9}$$

and, accordingly with Andreini and Da Soghe [20],

$$C_{d\_IntCrFlow} = (1 + c_2 \cdot c_3^{c_4 \cdot MVR^{\gamma}}) \tag{10}$$

The five coefficients of the correlation were calculated minimizing the RMS through the interpolation, with the expression 10, of the values of discharge coefficients extracted from the CFD: a mean relative error of 1.6% and a maximum of 4.5% was computed, with a standard deviation of 1.2% (i.e. 95% of the $C_d$ predicted when using the correlation leads to an error lower than 3% with respect to the CFD data set). Table 3 reports the suggested correlation coefficients.

In Fig. 17, the values of the $C_d^{**}$ values predicted through the correlation are compared with those predicted by the CFD for all geometries and operating conditions considered in this paper. The figure shows that a quite good agreement between CFD and correlation is achieved for all geometries and operating conditions.

## Verification of Correlation Accuracy

**Comparison With Literature Experimental Data.** To further prove its reliability, the correlation predictions have been compared with the experimental data of Gritsch and coworkers [9]. In the mentioned contribution, measurements of discharge coefficients for several configurations of cylindrical hole geometries are presented. These comprise holes characterized by angles of inclination 90 and length-to-diameter ratio 3 which are tested over a

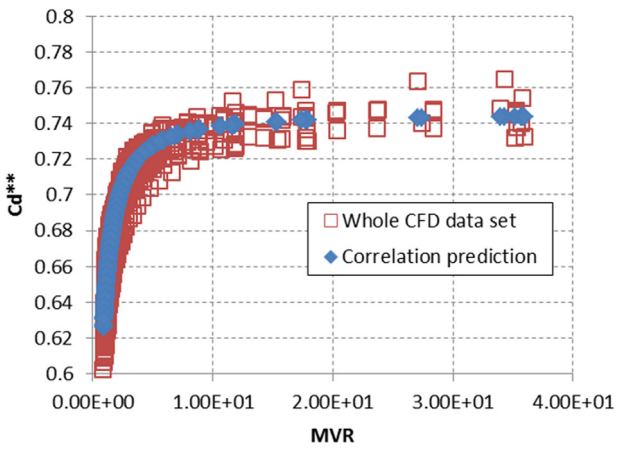


**Fig. 17 $C_d^{**}$ over *MVR* parameter distribution: comparison among correlation prediction and whole CFD data set (i.e., all geometries and related operating conditions**

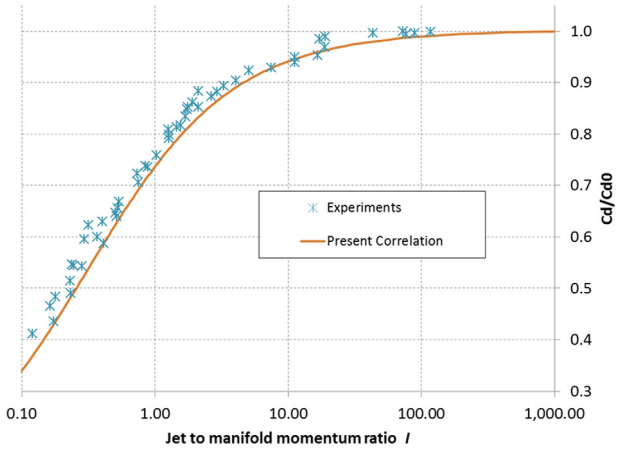


**Fig. 18 Comparisons among correlation predictions and Gritsh et al. experimental data [9]: effects of jet-to-manifold flow momentum ratio on $C_d$ distribution**

wide range of engine like conditions. The mentioned experimental data consists in a valuable reference to validate the developed correlation. First, the effect of the jet-to-manifold flow momentum ratio $(I = (\rho \cdot v^2)_{jet}/(\rho \cdot v^2)_{manifoldflow})$ is considered. The discharge coefficients are normalized by the plenum-to-plenum discharge coefficient (i.e., the Cd evaluated in case of MVR higher than 1000) at the same pressure ratio and then plotted versus the jet-to-manifold flow momentum ratio $I$. The results of this analysis consists in the following Fig. 18.

From the graph, it emerges that the correlation mimics quite well the experimental data provided by Gritsch and coworkers [9]. To conclude the effect of manifold flow Mach number on the discharge coefficient is evaluated for different pressure ratio. In their contribution, Gritsch et al. [9] calculate the isentropic mass flow rate (and then the hole discharge coefficient) using upstream total quantities (i.e. manifold total temperature and total pressure). Bearing in mind that in present contribution the isentropic mass flow rate is calculated using static quantities (i.e. manifold static temperature and static pressure), in order to properly compare the experimental data with the correlations predictions, the calculated Cd have to be scaled as follow:

$$C_{d\_tot} = C_d \cdot \frac{m_{is}}{m_{is\_tot}} \tag{11}$$

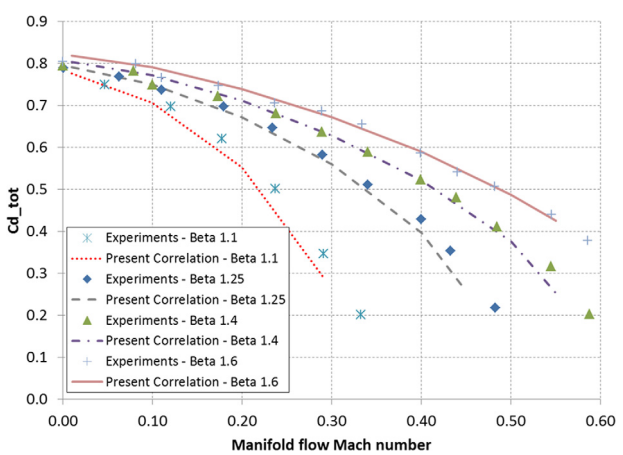


**Fig. 19 Comparisons among correlation predictions and Gritsch et al. experimental data [9]: effects of manifold flow Mach number on discharge coefficient**

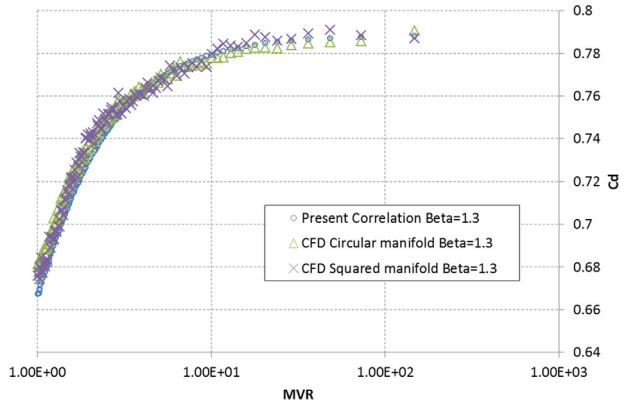


**Fig. 20 Comparisons among circular and squared supply manifold geometry**

where the $C_d$ is the holes discharge coefficient evaluated using the new correlation, $m_is$ is the isentropic mass flow rate calculated using static quantities and $m_{is\_tot}$ is the isentropic mass flow rate evaluated accordingly with Gritsch et al. [9]. Figure 19 reports the effect of manifold flow Mach number on the discharge coefficient evaluated for different pressure ratio.

From the figure, it emerges that a the correlation agrees quite well with the experimental data for all tested conditions. The most relevant discrepancies occur in case of low $\beta$ ratio for which the experimental errors are the highest (as reported by Gritsch et al. [9]). As the pressure ratio increase, the agreement among the correlation predictions and the experiments improves revealing the excellent job done by the correlation.

**Noncircular Supply Manifold.** In ACC systems, the feeding manifolds can sometime have a noncircular shape (in some cases a square arrangement is considered as shown in Fig. 1). In this section, the correlations predictions are compared with CFD in case of a square shaped manifold geometry. The analyzed geometry consists in a modification of the geometry labeled A for which only the manifold shape is changed. The manifold inlet area was kept the same of that one related to geometry A. The results of this analysis are reported in Fig. 20 in case of $\beta = 1.3$.

As shown by the figure, the correlation is able to confidently predict the hole's discharge coefficient in case of squared pipe, as the $C_d$ distribution seems slightly affected by the manifold geometry shape.

## Conclusions and Perspectives for Future Work

A three-dimensional CFD analysis was performed in order to investigate the aerodynamic losses of holes array located on manifolds; the investigation was carried out with the use of a test matrix of numerical simulations, which allowed to analyze several geometries typically implemented in ACC systems, over a wide range of fluid-dynamics conditions.

The analysis takes into account several geometrical aspects, i.e., the number of impinging holes, their length-to-diameter ratio, the holes spacing and the manifold diameter.

The CFD results were preliminary validated by the data obtained through a dedicated experimental campaign carried out on a test rig at the Department of Energy Engineering of the University of Florence.

The study led to the development of an empirical correlation for the prediction of the discharge coefficient: it expresses the $C_d$ of each hole as a function of the ratio between the hole and the manifold mass velocity, the hole length-to-diameter ratio and the local value of the $\beta_L$ ratio.

The correlation was deduced from the analysis of the discharge coefficients extracted from the numerical simulations; it

reproduces the trend of the $C_d$ with an average relative error of 1.6% and a maximum error of 4.5% over the whole range of fluid-dynamics and geometrical conditions. Finally, the study has revealed that the effects of the holes axial displacement has a weak effect on the discharge coefficient so that this parameter has not been taken into account for the $C_d$ correlation.

The correlation was then validated through the experimental data of Gritsch and coworkers [9]. This validation study proves the excellent job done by the correlation.

Finally, a preliminary study has been conducted, by means of CFD, in order to point out if the correlation is able to confidently predict the discharge coefficient behavior in case of noncircular feeding pipe geometry. The analysis reveals that the correlation well agrees with the CFD in case of squared manifold geometry as the feeding pipe shape has a slight impact on the $C_d$.

Although the correlation has been developed focusing on ACC systems, it could be useful for other gas turbine applications based on impingement cooling, i.e., airfoil leading edge and trailing edge impingement cooling (Han et al. [25], Halila et al. [2]), end-wall cooling (Halila et al. [2]) and so on. In this way, the authors recognize that the impact on the discharge coefficient the external flow should be accounted for to provide a correlation for more general applications. This will be done by the authors in the near future defining new multiplying correction term ($C_{d\_ExtCrFlow}$) function of the external cross flow.

## Nomenclature

$A$ = tube internal area $(mm^2)$
$Cd$ = discharge coefficient
$Cd^*$ = scaled discharge coefficient
$Cp$ = pressure coefficient
$d$ = cooling hole diameter $(mm)$
$D$ = tube internal diameter $(mm)$
$MV$ = mass velocity $\rho v$ $(kg/sm^2)$
$MVR$ = mass velocity ratio $(\rho v)_j/(\rho v)_c$
$L$ = tube length $(mm)$
$\dot{m}$ = mass flow rate $(kg/s)$
$Ma$ = Mach number
$P$ = pressure $(Pa)$
$Re$ = Reynolds number $Re = \frac{\rho \cdot v \cdot D}{\mu}$
$R$ = gas constant $(J/kgK)$
$S$ = pitch $(mm)$
$t$ = wall thickness $(mm)$
$T$ = temperature $(C)$
$v$ = mean velocity $(m/s)$

## Acronyms

$Me$ = million elements
$RMS$ = root mean square
$ACC$ = active clearance control
$Pt_1$ = total pressure at measure point 1

## Greek

$\beta$ = global P ratio(P@manifold inlet/P@outlet)
$\beta_L$ = local pressure ratio
$\mu$ = air viscosity $(kg/ms)$
$\rho$ = air density $(kg/m^3)$
$\gamma$ = heat capacity ratio

## Subscripts

$av$ = averaged value
$c$ = main channel
$d$ = discharge coinditions
$i$ = $i$th pressure taps
$is$ = isentropic
$j$ = jet hole
$s$ = static
$t$ = total
$x$ = streamwise direction

## References


[1] Justak, J. F., and Doux, C., 2009, "Self-Acting Clearance Control for Turbine Blade Outer Air Seals," Proceedings of the ASME Turbo Expo, Orlando, FL, June 8–12, ASME Paper No. GT2009-59683.
[2] Halila, E., Lenahan, D., and Thomas, T., 1982, "High Pressure Turbine Test Hardware," NASA Report No. CR-167955.
[3] Beck, B., and Fasching, W., 1982, "CF6 Jet Engine Performance Improvement - Low Pressure Turbine Active Clearance Control," NASA Report No. CR-165557.
[4] Lefebvre, A., 1998, *Gas Turbine Combustion*, Taylor & Francis, New York.
[5] Hay, N., and Lampard, D., 1998, "Discharge Coefficient of Turbine Cooling Holes: A Review," ASME J. Turbomach., **120**, pp. 314–319.
[6] Gritsch, M., Schulz, A., and Wittig, S., 1998, "Method of Correlating Discharge Coefficient of Film-Cooling Holes," AIAA J., **36**, pp. 976–980.
[7] Gritsch, M., Schulz, A., and Witting, S., 1999, "Effect of Internal Coolant Crossflow Orientation on the Discharge Coefficient of Shaped Film Cooling Holes," Proceedings of the ASME Turbo Expo, Indianapolis, IN, June 7–10, ASME Paper No. 99-GT-40.
[8] Rowbury, D., Oldfield, M., and Lock, G., 2001, "A Method for Correlating the Influence of External Crossflow on the Discharge Coefficients of Film Cooling Holes," ASME J. Turbomach., **123**, pp. 258–265.
[9] Schulz, A., Gritsch, M., and Wittig, S., 2001, "Effect of Crossflows on the Discharge Coefficient of Film Cooling Holes With Varying Angles of Inclination," Proceedings of the ASME Turbo Expo, New Orleans, LA, June 4–7, ASME Paper No. 2001-GT-0134.
[10] Thole, K., Smith, J., and Miller., A., 1997, "Effect of a Cross-Flow at the Entrance to a Film-Cooling Hole," ASME J. Fluids Eng., **119**, pp. 533–541.
[11] Hay, N., Lampard, D., and Khaldi, A., 1994, "The Coefficient of Discharge of 30 Inclined Film Cooling Holes With Rounded Entries or Exits," Proceedings of the ASME Turbo Expo, The Hague, Netherlands, June 13–16, ASME Paper No. 94-GT-180.
[12] Goodro, M., Park, J., Ligrani, P. M., Fox, M., and Moon, H.-K., 2007, "Effects of Mach Number and Reynolds Number on Jet Array Impingement Heat Transfer," Int. J. Heat Mass Transfer, **50**(1), pp. 367–380.
[13] Park, J., Goodro, M., Ligrani, P. M., Fox, M., and Moon, H.-K., 2007, "Separate Effects of Mach Number and Reynolds Number on Jet Array Impingement Heat Transfer," ASME J. Turbomach., **129**(2), pp. 269–280.
[14] Goodro, M., Park, J., Ligrani, P. M., Fox, M., and Moon, H.-K., 2008, "Effect of Hole Spacing on Spatially-Resolved Jet Array Impingement Heat Transfer," Int. J. Heat Mass Transfer, **51**(25–26), pp. 6243–6253.
[15] Goodro, M., Park, J., Ligrani, P. M., Fox, M., and Moon, H.-K., 2009, "Effect of Temperature Ratio on Jet Array Impingement Heat Transfer," ASME J. Heat Transfer, **131**(1), p. 012201.
[16] Goodro, M., Park, J., Ligrani, P. M., Fox, M., and Moon, H.-K., 2010, "Mach Number, Reynolds Number, Jet Spacing Variations: Full Array of Impinging Jets," AIAA J. Thermophys. Heat Transfer, **24**(1), pp. 133–144.
[17] Andreini, A., Bonini, A., Caciolli, G., Facchini, B., and Taddei, S., 2010, "Numerical Study of Aerodynamic Losses of Effusion Cooling Holes in Aero-Engine Combustor Liners," Proceedings of the ASME Turbo Expo, Glasgow, UK, June 14–18, ASME Paper No. GT2010-22942.
[18] Ahmed, F., Weigand, B., and Meier, K., 2010, "Heat Transfer and Pressure Drop Characteristics for a Turbine Casing Impingement Cooling System," Proceedings of the ASME International Heat Transfer Conference, Washington, DC, August 8–13, ASME Paper No. IHTC14-22817.
[19] Ahmed, F., Tucholke, R., Weigand, B., and Meier, K., 2011, "Numerical Investigation of Heat Transfer and Pressure Drop Characteristics for Different Hole Geometries of a Turbine Casing Impingement Cooling System," Proceedings of the ASME Turbo Expo, Vancouver, Canada, June 6–10, ASME Paper No. GT2011-45251.
[20] Andreini, A., and DaSoghe, R., 2011, "Numerical Characterization of Aerodynamic Losses of Jet Arrays for Gas Turbine Applications," ASME Paper No. GT2011-46212.
[21] DaSoghe, R., Maiuolo, F., Tarchi, L., Micio, M., and Facchini, B., 2011, "Discharge Coefficient Characterization of Jet Array Impingement Holes for an Active Clearance Control System," Proceedings of the ETC, Paper No. ETC2011-252.
[22] Andreini, A., Da Soghe, R., Facchini, B., Maiuolo, F., Tarchi, L., and Coutandin, D., 2012, "Experimental and Numerical Analysis of Multiple Impingement Jet Arrays for an Active Clearance Control System," ASME Paper No. GT2012-68791.
[23] CFX, A., 2011, *Solver Theory Guide*. Ansys, Inc., Canonsburg, PA.
[24] Lichtarowicz, A., Duggins, R., and Markland, E., 1965, "Discharge Coefficients for Incompressible Non-Cavitating Flow Through Long Orifices," J. Mech. Eng. Sci., **7**(2), 210219.
[25] Han, J. C., Dutta, S., and Ekkad, S., 2000, *Gas Turbine Heat Transfer and Cooling Technology*, Taylor & Francis, New York.